Received 10 March 2020; revised 31 March 2020; accepted 6 April 2020. Date of publication 9 April 2020; date of current version 13 May 2020.

Digital Object Identifier 10.1109/OJCOMS.2020.2986874

Hybrid NOMA and ZF Pre-Coding Transmission for Multi-Cell VLC Networks

MAHMOUD WAFIK ELTOKHEY[1] (Member, IEEE), MOHAMMAD ALI KHALIGHI[1] (Senior Member, IEEE), ABDALLAH S. GHAZY[2], AND STEVE HRANILOVIC[2] (Senior Member, IEEE)

[1]Aix Marseille University, CNRS, Centrale Marseille, Institut Fresnel, Marseille, France

[2]Department of Electrical and Computer Engineering, McMaster University, Hamilton, ON L8S 4K1, Canada

CORRESPONDING AUTHOR: M. A. KHALIGHI (e-mail: ali.khalighi@fresnel.fr)

This work was supported in part by the European Union's Horizon 2020 Research and Innovation Programme under the Marie Skłodowska-Curie under Grant Agreement No. 764461 (VisIoN).

ABSTRACT Though visible-light communication (VLC) channels are contained by opaque boundaries, they present unique challenges in the development of multi-user/multi-cell scenarios. In this paper, two hybrid transmission schemes are proposed for managing multiple users in multi-cell VLC networks. The proposed schemes are based on using non-orthogonal multiple access (NOMA) in the network access points (APs), while applying zero-forcing (ZF) pre-coding to the cell edge users' signals, which are cooperatively broadcast from the APs. The proposed approach allows a reduction of the inter-cell interference affecting the cell-edge users thanks to ZF pre-coding, while dealing with inter-user interference for cell-center users via NOMA signaling. Considering different transmission scenarios, we show the improvement in the network total achievable data rate as well as fairness, as compared to conventional NOMA. For example, for a typical scenario considered, an improvement of up to 39% in total achievable rate and up to 112% in the network fairness is achieved. The proposed approach also presents a clear advantage over the conventional ZF pre-coding, for which the maximum number of users is constrained to the number of APs.

INDEX TERMS Visible light communications, multi-user networks, non-orthogonal multiple access, pre-coding.

I. INTRODUCTION

VISIBLE light communications (VLC) is regarded as a strong candidate for providing high-speed wireless access in indoor scenarios, due to the huge available unlicensed bandwidth, reliance on the existing light-emitting diode (LED)-based lighting infrastructure, insensitivity to radio-frequency interference, and inherent security [1]–[3]. In order to address network coverage and user mobility in large indoor spaces, recent research has in particular focused on developing appropriate multiple access (MA) techniques in the VLC context. We focus in this paper on MA management in downlink (DL) transmission in a VLC network. Within this context, considerable attention has been devoted to non-orthogonal multiple access (NOMA), which is also a serious candidate for the future fifth-generation (5G) cellular networks due to its better performance as compared with the conventional orthogonal MA schemes [4]–[7].[1] Through power-domain NOMA (that we will simply refer to as NOMA), multiple user signals are multiplexed in the DL in the power domain at the access point (AP) using superposition coding. At the receiver (Rx), successive interference cancellation (SIC) is performed to recover the signal of each user while trying to minimize the interference arising from the other users [9]. In the 5G context, the potential limitations of NOMA have been the subject of extensive research in the past few years, mainly as compared to orthogonal MA schemes [10]. In VLC networks, however, NOMA appears to be particularly promising due

1. Note that, concerning the uplink, which could be realized using infrared transmission, carrier-sense MA with collision avoidance (CSMA/CA) protocol can be used, as suggested in [8].

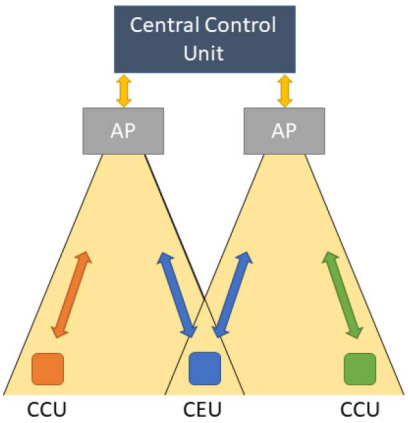

FIGURE 1. Illustration of a cellular VLC network highlighting a central control unit, two APs, two CCUs, and a CEU.

to the small-cell deployment of the network and the need to handle a relatively small number of users. Moreover, the typically high signal-to-noise ratio (SNR) in indoor VLC scenarios and slowly changing channel conditions with typical user movements, make NOMA signaling of particular interest [9], [11], [12]. For instance, a comparative study of orthogonal frequency-division MA (OFDMA) [13] and orthogonal frequency-division multiplexing (OFDM)-based NOMA was presented in [9], [14] for the case of a single-cell scenario, where the advantage of the latter in terms of network throughput was demonstrated, in particular, for an increased number of users. In a recent work, we compared the performances of NOMA and OFDMA for the case of large indoor scenarios, and highlighted the advantage of the former in terms of network throughput [15].

Most previous work has centered on a single-cell VLC network [9], [14], [16]. Here, we consider a relatively large-space, multi-user indoor scenario, where multiple LED luminaires can serve as separate APs, each one potentially handling several users in its coverage area (i.e., cell). This is the case, for example, for a relatively large office or a conference hall. Figure 1 illustrates the principle of such a multi-cell network. Therein, users are handled differently depending on whether they are located at "cell centers" or at "cell edges". A central control unit connects the APs and has the task of information exchange and coordination between them. It also defines the cell boundaries, and consequently, specifies cell-center users (CCUs) and cell-edge users (CEUs). The APs, in turn, are responsible for identifying the channel information for all users, and forwarding it to the central control unit.

In such a cellular scenario, there are two primary types of interference: the inter-user interference (IUI) resulting from the interference between the users within a cell, and the inter-cell interference (ICI) resulting from the interference arising from neighboring cells. In particular, handling CEUs that are subject to intense ICI becomes a delicate task. In [17], [18], fractional frequency reuse is used to manage the ICI of CEUs by dividing the bandwidth into sub-bands that are assigned according to the respective locations of the users within the cells. The main drawback is the decrease in the network spectral efficiency. The use of red, green, and blue (RGB) LEDs was considered for ICI mitigation in [19], where different color resources are allocated to different cells. The use of RGB LEDs limits the applicability of the proposed technique and additionally impacts illumination performance of the system (e.g., color rendering). Angle-diversity receivers were studied in [20], where several photo-detectors (PDs) with different orientations are employed for ICI mitigation. Similar to the previous approaches, the need for this specific Rx architecture limits its widespread applicability. On the other hand, a few recent works studied NOMA-based multi-cell signaling. For instance, [18] and [21] proposed ICI mitigation through frequency reuse at the cost of decreased spectral efficiency. Also, [22] considered transmitting the same signal by all APs, hence eliminating the need for ICI mitigation, but at the cost of increased average number of SIC steps at the Rxs and increased IUI.

When multiple LED luminaires serve as APs, the ensemble of APs and a given Rx form a multiple-input single-output (MISO) structure (assuming every Rx uses a single PD). In such a case, MA via linear zero-forcing (ZF) pre-coding at the APs allows removal of MA interference at the Rxs [23]–[26]. An extension of this idea to the general case of user pre-coding with different optimization criteria was proposed in [27], and termed coordinated broadcasting. ZF pre-coding along with user scheduling was also considered in multi-cell VLC networks for ICI mitigation in [28]. However, ZF-based linear pre-coding can only be used when the instantaneous number of Rxs does not exceed the number of APs, which can be quite constraining in practice. Some other works for RF cellular networks studied other types of NOMA pre-coding with the goal of interference mitigation, see for instance, [29], [30]. However, these techniques cannot be applied to VLC systems due to the constraint of needing positive and real signals for intensity modulation with LEDs.

In this paper, we present two MA schemes for multi-user multi-cell VLC networks which combine NOMA for the management of IUI and MISO ZF pre-coding to manage ICI. The main idea is to allow CCUs to reduce IUI through SIC detection in a NOMA scheme, while allowing CEUs to remove ICI based on ZF pre-coding. Compared to other linear pre-coding schemes, ZF pre-coding offers simplicity while providing good performance at high SNR, which is typically the case for indoor VLC networks [31]–[33]. More specifically, in this *hybrid* approach, termed here *NOMA-ZFP*, the CCUs in a given cell are associated with the corresponding AP, and NOMA signaling is applied to manage them. The signals for the CEUs are first pre-coded and then broadcast from the neighboring APs as the last-priority user in the NOMA scheme, i.e., by allocating to them the smallest portion of the transmit power. At the Rx side, CEUs detect their signals after removing the interference arising from the CCUs present in the neighboring cells using SIC. This approach provides efficient multi-user (MU) detection

with reasonable complexity since the number of users relying on either NOMA or ZF pre-coding is reduced. Our results show that this approach results in a performance improvement as compared to the case where either NOMA or MISO ZF pre-coding alone are used to manage all users, especially for increased user density within the cells. Moreover, this approach potentially reduces the number of handovers in the case of mobile users because CEUs are managed without a requirement to switch the AP (compared to the case where a CEU is handled by the AP from which it receives the strongest signal). Compared to the aforementioned solutions, our proposed NOMA-ZFP schemes do not sacrifice spectral efficiency to mitigate ICI and do not rely on the use of any specific transmitter (Tx) or Rx opto-electronics. Numerical results presented here demonstrate the advantage of NOMA-ZFP in terms of sum-rate and fairness as compared with the basic NOMA in different link scenarios. In summary, the advantages of the proposed hybrid NOMA-ZFP schemes include:

- improving the performance of NOMA by decreasing the effective number of users within each cell, i.e., the number of users handled (only) with NOMA;
- suppressing IUI for CEUs through SIC detection of the corresponding CCUs' signals, and removing ICI of the other CEUs signals through ZF pre-coding;
- serving CEUs while dedicating a relatively small portion of the APs' powers to them;
- potentially reducing the number of handovers for moving users.

Note that what makes the proposed hybrid scheme particularly suitable for VLC networks (as compared with RF cellular networks) is that these networks should typically handle a low number of users in their coverage area. As a result, the assumption of having the number of CEUs smaller than or equal to the number of APs (which is the condition for using ZF pre-coding) is rather reasonable.

The remainder of the paper is organized as follows. Section II provides the description of the considered VLC network and a brief presentation of ZF pre-coding and NOMA techniques and their mathematical formulation. Section III introduces the proposed hybrid NOMA-ZFP scheme. Numerical results are presented in Section IV to study the performance of the proposed scheme. Lastly, the paper concludes in Section V.

Notation: Throughout the paper, matrices are represented with bold-face upper-case letters (e.g., $\boldsymbol{A}$) and vectors with bold-face lower-case letters ($\boldsymbol{a}$). Also, diag($\boldsymbol{a}$) denotes a diagonal matrix with its diagonal being the entries of the vector $\boldsymbol{a}$, det($\boldsymbol{A}$) stands for the determinant of $\boldsymbol{A}$, and $\boldsymbol{I}$ represents the identity matrix.

II. SYSTEM MODEL, ASSUMPTIONS, AND MA APPROACHES

A. GENERAL ASSUMPTIONS

We consider intensity modulation with direct detection due to the use of LEDs at the Tx. Let N_t denote the number of APs, located at the ceiling, which manage a total number of N_r Rxs within their coverage area. In order to consider a general case, assume the use of a positive-intrinsic-negative (PIN) PD with an optical concentrator at each Rx. Let AP_i, $i = (1, 2, \ldots, N_t)$, and U_j, $j = (1, 2, \ldots, N_r)$, denote the i^{th} AP and the j^{th} user, respectively. The channel gain for the link between AP_i and U_j is denoted by h_{ij}. Assuming a Lambertian pattern for the LED luminaires and that the line-of-sight (LOS) component is not blocked or shadowed and dominates the non-LOS components, the channel gains have the form (see [1], [34]–[36]):

$$h_{ij} = \mathcal{R}\,\mathcal{S}\,\frac{(m+1)\,A_j}{2\pi\, l_{ij}^2}\cos^m(\phi_{ij})\cos(\theta_{ij}), \tag{1}$$

where ϕ_{ij} refers to the angle of emission with respect to AP_i, θ_{ij} refers to the incident angle with respect to U_j, and l_{ij} denotes the link distance between AP_i and U_j. Also, $\mathcal{R}$ is the PD responsivity, assumed to be the same for all Rxs, $\mathcal{S}$ is the LED conversion efficiency, and m the Lambertian order, assumed to be the same for all LED luminaires. In addition, A_j is the j^{th} Rx collection area, which is given by [37]:

$$A_j = \frac{q_j^2}{\sin^2(\theta_{cj})} A_{\text{PD}_j}, \tag{2}$$

with A_{PD_j} denoting the Rx active photo-detection area, q_j the optical concentrator refractive index, and θ_{cj} the Rx field of view (FOV) corresponding to U_j. Without loss of generality, we hereafter assume that all PDs are identical and have area $A_j = A$.

B. MISO ZF PRE-CODING

In NOMA-ZFP, multiple APs and a given Rx are considered as a MISO structure. Based on this formulation, linear ZF pre-coding is performed at the APs on the users' signals that results in the suppression of interference from other users at each Rx. To do this, the channel state information (CSI) of all underlying channels must be estimated at each Rx (for instance, based on the transmission of some pilot symbols from the APs in the DL), and sent back to the APs (in the uplink). This CSI is then used by the APs to calculate the appropriate ZF pre-coding matrix [25].

At AP_i, the j^{th} user's symbol d_j is multiplied by a pre-coding weight w_{ij}. Combining all weighted symbols for N_r users (excluding the DC bias), we obtain the transmitted signal x_i

$$x_i = \sum_{j=1}^{N_r} w_{ij}\, d_j. \tag{3}$$

The received signal at U_j after removing the DC offset is

$$r_j = \sum_{i=1}^{N_t} x_i h_{ij} + z_j, \tag{4}$$

where z_j is the noise sample, considered as Gaussian distributed with variance σ_n^2, which models the impact of

ambient noise and the Rx pre-amplifier thermal noise. Define $\boldsymbol{d} = [d_1, \ldots, d_{N_r}]$, $\boldsymbol{x} = [x_1, \ldots, x_{N_t}]$, $\boldsymbol{r} = [r_1, \ldots, r_{N_r}]$, $\boldsymbol{h}_j = [h_{1j}, \ldots, h_{N_t j}]^T$, and $\boldsymbol{w}_j = [w_{1j}, \ldots, w_{N_t j}]^T$. Equation (4) can be rewritten as

$$r_j = \boldsymbol{h}_j^T \boldsymbol{x} + z_j = \boldsymbol{h}_j^T \boldsymbol{w}_j d_j + \sum_{k \neq j} \boldsymbol{h}_j^T \boldsymbol{w}_k d_k + z_j, \tag{5}$$

where $(\cdot)^T$ denotes transposition. In (5), the first term on the right side contains the desired signal and the second term refers to the ICI from the other users. In matrix form,

$$\boldsymbol{r} = \boldsymbol{H}^T \boldsymbol{W} \boldsymbol{d} + \boldsymbol{z}, \tag{6}$$

where $\boldsymbol{H} = [\boldsymbol{h}_1^T, \ldots, \boldsymbol{h}_{N_r}^T]^T$ and $\boldsymbol{W} = [\boldsymbol{w}_1^T, \ldots, \boldsymbol{w}_{N_r}^T]^T$ denote the network channel matrix and the pre-coding weight matrix, respectively, both of dimension $(N_r \times N_t)$, and $\boldsymbol{z} = [z_1, \ldots, z_{N_r}]$ is the noise vector at the Rxs. As mentioned previously, for simplicity, linear ZF pre-coding [25] is considered for the calculation of $\boldsymbol{W}$ yielding

$$\boldsymbol{W} = \boldsymbol{H}^T (\boldsymbol{H}\boldsymbol{H}^T)^{-1} \operatorname{diag}(\boldsymbol{\gamma}). \tag{7}$$

The diagonal entries $\gamma_j > 0$ (that can be considered as the coefficients of parallel sub-channels) determine the SNR at user U_j, and are determined based on a performance metric (e.g., throughput maximization in [25]). The SNR at U_j is defined as

$$\mathrm{SNR}_{\mathrm{ZFP},U_j} = \frac{\left(\boldsymbol{h}_j^T \boldsymbol{w}_j\right)^2}{\sigma_n^2} = \frac{\gamma_j^2}{\sigma_n^2}. \tag{8}$$

The upper bound on the achieved rate for U_j follows as

$$R_{\mathrm{ZFP},U_j} = \frac{B}{2} \log_2\left(1 + \mathrm{SNR}_{\mathrm{ZFP},U_j}\right) \quad \text{(bps)}, \tag{9}$$

where B is the system (Tx-Rx) bandwidth (BW), and data rate is measured in bits per second (bps). In fact, (9) has the implicit assumption that signal modulation at the Tx is based on DC-biased optical OFDM (DCO-OFDM), where due to the Hermitian symmetry constraint, we have a loss of factor two in the spectral efficiency [1]. Note that this also applies to the case of the (bandpass) carrierless amplitude and phase (CAP) modulation [38].

C. NOMA SIGNALING

NOMA is based on multiplexing users' signals in the power domain at the Tx using superposition coding [5]. At the Rx side, SIC is performed for signal detection in order to minimize the interference arising from the other users' signals [9]. An important point to consider is that in order to provide a homogeneous level of performance to all users, regardless of the channel conditions, the power allocation (PA) among users must be carefully selected. To accomplish this, at the AP users are ranked based on their channel gains, and their signals are assigned adequate PA weights accordingly; i.e., users with lower channel gains are allocated a higher power. At the Rx, users with lower channel gains decode their data before the others. Initially, SIC is performed to (ideally) cancel the interference from already-detected signals (i.e., users with lower channel gains). The corresponding user's signal is then detected while considering the other remaining undesired signals as interference. To perform SIC, the CSI of the corresponding users is required. Considering AP_i as Tx and assuming perfect CSI knowledge at all users, the received signal at U_j is given by [11][2]:

$$r_j = a_{ij} \sqrt{P_e}\, h_{ij}\, d_j + \sum_{k=1}^{j-1} a_{ik} \sqrt{P_e}\, h_{ij}\, d_k + \sum_{k=j+1}^{N_r} a_{ik} \sqrt{P_e}\, h_{ij}\, d_k + z_j, \tag{10}$$

where P_e and a_{ij} represent the total transmitted electrical power (excluding the DC offset) and the PA weight by AP_i for U_j, respectively. The first term in (10) represents the desired signal for U_j, the second term denotes the interference that could be (ideally) removed using SIC (for $k < j$), and the third term represents the residual interference after SIC (for $k > j$). For the first user, i.e., the user with the highest channel gain, the detection is done directly. For the succeeding users, SIC detection is performed before signal detection using the CSI of the preceding users.

The performance of NOMA depends in particular on the PA to different users at the AP, which has been investigated in the recent literature. Though other PA scheme have been proposed recently which aim to maximize total throughput [11], [18], [39], [40], in this work due to its low complexity, a static PA approach is considered which consists of sorting the users based on their channel gains and then assigning them power by considering a certain PA coefficient, regardless of the actual channel gains [12]. Using static power allocation for AP_i and U_j,

$$a_{ij}^2 = \alpha\ a_{ij-1}^2, \tag{11}$$

where α is the PA factor, representing the ratio between the allocated power to a given user and that to the preceding one in the decoding order. Clearly, $\sum_{j=1}^{N_r} a_{ij}^2 = 1$, to ensure a fixed normalized electrical transmit power [14]. With this formulation, the electrical signal-to-interference-plus-noise ratio (SINR) for U_j is given by:

$$\mathrm{SINR}_{\mathrm{NOMA},U_j} = \frac{h_{ij}^2 P_e\, a_{ij}^2}{I_{\mathrm{ICI}} + h_{ij}^2 P_e \sum_{k>j} a_{kj}^2 + \sigma_n^2}, \tag{12}$$

where I_{ICI} denotes interference due to ICI. The upper bound on the achieved rate for U_j is then calculated as follows [9]:

$$R_{\mathrm{NOMA},U_j} = \frac{B}{2} \log_2\left(1 + \mathrm{SINR}_{\mathrm{NOMA},U_j}\right) \quad \text{(bps)}, \tag{13}$$

where again the assumption of DCO-OFDM signaling is made.

2. Note that the dependence of r_j on AP_i is implicit. This allows us to use the same notation for the case of hybrid schemes, see Section III-A.

D. CONSIDERED NOMA SCHEMES

This work considers two NOMA schemes, which differ in the way of associating CEUs to the APs, inspired by [41]. In the first scheme, denoted NOMA-A, CEUs are associated with all APs that cover its location, while implicitly assuming that each CEU can separate the signals sent from the different associated APs (see [41]). Ideally, this results in less interference for CEUs, since they can use SIC to decrease the interference arising from the signals received from the different APs. However, this comes at the expense of increased network complexity since each CEU may require the CSI of other users in the corresponding cells (depending on the decoding order). In addition, this increases the user density for the APs [41]. In the second scheme, denoted NOMA-B, each CEU is associated with only the AP that corresponds to the strongest channel gain. This results in decreased cell density at the APs and decreased network complexity because CEUs will need the CSI of users of only one cell. However, CEUs in NOMA-B suffer from increased interference, as compared to NOMA-A, arising from the received signals of the other APs [41]. With a higher complexity compared with NOMA-B, NOMA-A mostly offers improved performance in terms of both sum-rate and fairness.

III. HYBRID NOMA-ZFP

A. CONCEPT

This section introduces the proposed hybrid NOMA-ZFP approach for a multi-cell VLC network, which reduces IUI for CCUs and ICI for CEUs. Firstly, cell boundaries are defined, before the central control unit (see Fig. 1) classifies the existing users into CCUs (located in the coverage area of only one AP) and CEUs (located within the coverage areas of more than one AP). This is done based on the CSI of all users and according to a predefined minimum threshold channel gain [41], which is set to 9.74×10^{-7} here, corresponding to a 2 m cell radius. The signals from CCUs are coordinated by NOMA by the corresponding APs. Then, ZF pre-coding is employed for the CEU signals, where the resulting signal is broadcast by all neighboring APs. To accomplish this, the ensemble of CEUs is treated as a single "compound user" in the NOMA scheme while allocating to them a relatively low power. Figure 2 shows an illustration of the proposed hybrid NOMA-ZFP scheme for the case of a four-cell network.

At the Rx side, the signal of CCUs will be marginally impacted by the interference arising from the CEUs as a relatively small portion of the power is allocated to CEUs. On the other hand, CEUs will detect their desired signals after subtracting the CCUs' signals using SIC, assuming that the CSI of these latter is provided for CEUs.[3] It is important to mention that in the application of ZF pre-coding in NOMA-ZFP, the number of CEUs must not exceed the number of related APs. Notice that this constraint is more reasonable than in earlier MISO ZF pre-coding approaches [23]–[27], which require more luminaires than users. Note that in the cases where the number of CEUs is larger than the number N_t of APs, N_t CEUs will be handled by ZFP and the remaining ones by NOMA (along with the CCUs). Obviously, the CEUs handled by NOMA will suffer from a larger ICI in this way.

Let $N_{\mathrm{CCU},i}$ and N_{CEU} denote the number of CCUs in the i^{th} cell and the total number of CEUs in the network, respectively. Also, let $a^2_{\mathrm{CCU},i}$ and $a^2_{\mathrm{CEU},i}$ denote the total allocated portion of power to CCUs and to CEUs by AP_i, respectively, where $a^2_{\mathrm{CCU},i} + a^2_{\mathrm{CEU},i} = 1$. Then, the sum of PA weights for NOMA users cannot exceed $a^2_{\mathrm{CCU},i}$, that is,

$$\sum_{k=1}^{N_{\mathrm{CCU},i}} a^2_{ik} \leq a^2_{\mathrm{CCU},i}, \tag{14}$$

where a^2_{ik} is the NOMA PA weight used at AP_i for the k^{th} CCU. Similarly, the sum of the pre-coding weights per AP_i cannot be larger than $a_{\mathrm{CEU},i}\sqrt{P_e}$, that is,

$$\sum_{k=1}^{N_{\mathrm{CEU}}} |w_{ik}| \leq a_{\mathrm{CEU},i}\sqrt{P_e}. \tag{15}$$

Note that the conditions of (14) and (15) can also be considered to be related to the illumination constraints, determined by P_e. Also, note that in the case where no CCU is present in a cell (say, Cell i), the entire AP power is allocated to the CEUs, i.e., $a_{\mathrm{CEU},i} = 1$. Similarly, when there is no CEU in the network, the entire AP power is allocated to CCUs, i.e., $a_{\mathrm{CCU},i} = 1$.

Given that NOMA-ZFP scheme relies basically on the conventional NOMA, we provide in the following the formulation of the received signal based on what we presented in Section II-C. For user U_j with NOMA-ZFP signalling, the received signal is given by:

$$r_j = \sum_{i=1}^{N_t} \sum_{k=1}^{N_{\mathrm{CCU},i}+1} a_{ik}\sqrt{P_e}\, h_{ij}\, d_k + z_j, \tag{16}$$

where the AP_i handles the signal of $N_{\mathrm{CCU},i}$ CCUs plus that of all CEUs (remember that the signal for CEUs is transmitted as the highest decoding order user in the NOMA scheme). We can rewrite (16) in the following form:

$$r_j = \sum_{i=1}^{N_t} \sum_{k=1}^{N_{\mathrm{CCU},i}} a_{ik}\sqrt{P_e}\, h_{ij}\, d_k + \sum_{i=1}^{N_t} h_{ij}\, x_i + z_j, \tag{17}$$

where the first and the second terms represent the CCU and the CEU signals, respectively, and x_i is the CEUs ZF pre-coded signal sent by AP_i:

$$x_i = \sum_{k=1}^{N_{\mathrm{CEU}}} w_{ik}\, d_k, \tag{18}$$

where d_k is the k^{th} CEU symbol and w_{ik} is the corresponding ZF pre-coding weight. Note that, according to (15), x_i is

3. Note that throughout this paper, we assume ideal SIC based on perfect CSI at each Rx. The study of the impact of imperfect CSI on the network performance is beyond the scope of this work.

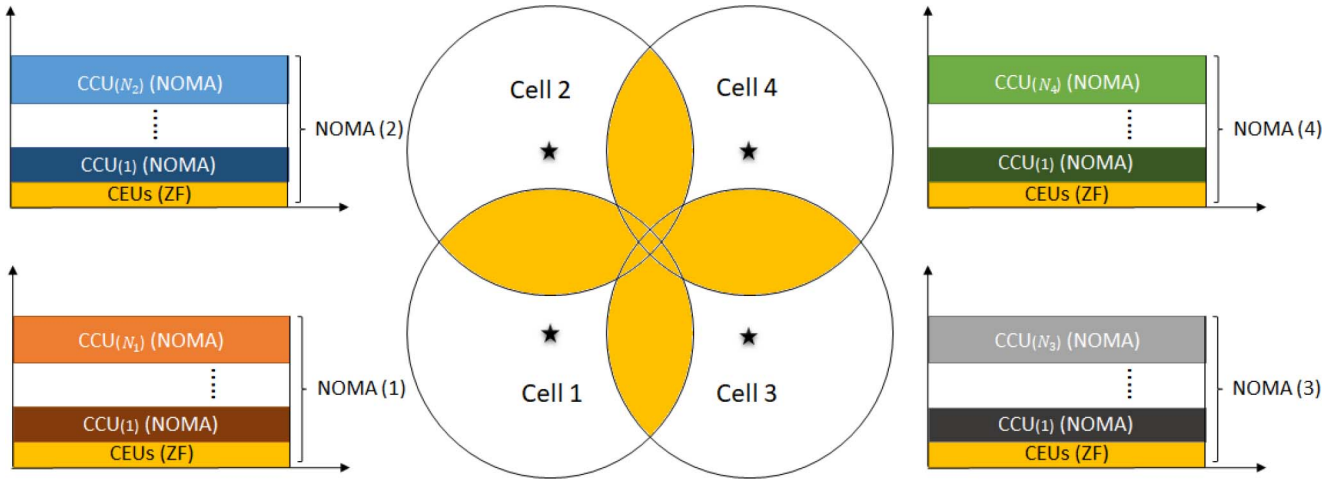

FIGURE 2. Illustration for the proposed hybrid NOMA-ZFP scheme for a 4-cell scenario. CEU locations correspond to the yellow colored areas, i.e., cell intersections. For instance, N_1 denotes the number of CCUs in Cell 1.

bounded by $a_{\text{CEU},i}\sqrt{P_e}$, which in fact sets a power limitation on CEUs. Using (5), we can write (17) as follows.

$$r_j = \sum_{i=1}^{N_t} \sum_{k=1}^{N_{\text{CCU},i}} a_{ik}\sqrt{P_e}\, h_{ij}\, d_k + \left(\boldsymbol{h}_j^T \boldsymbol{w}_j\, d_j + \sum_{k \neq j} \boldsymbol{h}_j^T \boldsymbol{w}_k\, d_k \right) + z_j. \tag{19}$$

If U_j is a CCU served by a given AP, the first term in (19) will include the desired signal and the ICI (here, the signals from other APs can be ignored as they are likely too weak), whereas the second term will represent the interference from CEU signals. On the other hand, if U_j is a CEU, the first term in (19) will represent the interference arising from CCUs (which is ideally removed by SIC), whereas the second term will include the desired signal (given that the interference of other CEUs is removed with ZF pre-coding).

There are several advantages of the proposed approach as compared to the conventional NOMA. First, it decreases the complexity of NOMA by reducing the number of processed users (i.e., number of CCUs plus one), which consequently decreases the CSI requirement and the computational complexity of SIC detection per NOMA transmission, while at the same time, allowing for a reduction of the interference level (IUI) for the CCUs. Secondly, it permits the use of a small portion of the APs power for serving CEUs through ZF pre-coding and signal broadcasting.

B. NOMA-ZFP SCHEMES

We propose and investigate two hybrid schemes, which differ in the criterion used for calculating the pre-coding weight matrix $\boldsymbol{W}$. From (6) and (19), the received signal vector of all CEUs in NOMA-ZFP is given by $\boldsymbol{r} = \boldsymbol{H}^T \boldsymbol{W}\boldsymbol{d} + \boldsymbol{z}$, where $\boldsymbol{W}$ is calculated from (7). Let us define vector $\boldsymbol{\mu}$ and matrix $\boldsymbol{A}$ as follows:

$$\boldsymbol{\mu} = \left[\mu_1, \ldots, \mu_{N_{\text{CEU}}}\right] = \left[\frac{\gamma_1}{\sigma_1}, \ldots, \frac{\gamma_{N_{\text{CEU}}}}{\sigma_{N_{\text{CEU}}}}\right], \tag{20}$$

$$\boldsymbol{A} = \text{abs}\left(\boldsymbol{H}^T (\boldsymbol{H}\boldsymbol{H}^T)^{-1}\right) \text{diag}(\boldsymbol{\sigma}), \tag{21}$$

such that

$$\boldsymbol{A}\boldsymbol{\mu} \leq \boldsymbol{F}_{\text{CEU}}; \quad \boldsymbol{\mu} \geq \boldsymbol{0}. \tag{22}$$

Here, $\boldsymbol{0}$ represents an all-zero vector, and

$$\boldsymbol{F}_{\text{CEU}} = \left[a_{\text{CEU},1}\sqrt{P_e}, \ldots, \; a_{\text{CEU},N_t}\sqrt{P_e}\right]. \tag{23}$$

In the first approach that we propose, termed *NOMA-ZFP-A*, the objective is to maximize the minimum achievable rate for CEUs that is a function of $\boldsymbol{\mu}$. This is referred to as the max-min fairness criterion in [25]:

$$\text{maximize} \quad \log_2(1 + \mu_{\min}^2), \tag{24}$$

where $\mu_{\min}$ corresponds to the smallest entry in vector $\boldsymbol{\mu}$, which can be obtained as:

$$\mu_{\min} = \frac{\min(\boldsymbol{F}_{\text{CEU}})}{\max(\boldsymbol{A}\,\boldsymbol{1})} \quad \text{subject to (22).} \tag{25}$$

By optimizing $\mu_{\min}$ from (24), the optimum $\boldsymbol{\mu}$ will equal $\mu_{\min}\boldsymbol{1}$, where $\boldsymbol{1}$ is the vector with all entries equal to one. In (25), the relationship of $\mu_{\min}$ to $\min(\boldsymbol{F}_{\text{CEU}})$ can be explained as to satisfy the lowest illumination constraint for CEU signals among all APs, and its relationship to $\max(\boldsymbol{A}\,\boldsymbol{1})$ is to guarantee the largest $\boldsymbol{W}$ for any AP transmission while satisfying (15). Note that our proposed solution is more general, compared with [25, eq. (28)]. Indeed, the solution of (24)-(25) accounts for the cases where APs have different power constraints on the ZF pre-coding weights (see (15)), by considering the minimum bound among all APs in the nominator of (25). In contrast, the solution proposed in [25] considers APs with the same power constraint on the pre-coding weights.

In the second approach, denoted by *NOMA-ZFP-B*, the target is the optimization of $\boldsymbol{\mu}$, subject to the constraint in (22), by maximizing the achievable throughput of CEUs [25]. Again, as CEU throughputs are function of their SNR (related to $\boldsymbol{\mu}$), the optimization is achieved by:

$$\text{maximize} \quad \log_2(\det(\boldsymbol{I} + \text{diag}(\boldsymbol{\mu} \odot \boldsymbol{\mu}))), \tag{26}$$

where $\odot$ denotes the Hadamard product. To avoid a non-concave objective function [23] while solving the problem as a standard determinant maximization, we simplify (26) to the following form, as considered in [25]:

$$\text{maximize} \quad \det(\boldsymbol{I} + \text{diag}(\boldsymbol{\mu})). \tag{27}$$

To solve (27), we use the CVX package [42], [43] for convex optimization, similar to [25]. After calculating $\boldsymbol{\mu}$, we can calculate $\boldsymbol{\gamma}$ from (20), and subsequently $\boldsymbol{W}$ can be obtained using (7).

IV. PERFORMANCE STUDY OF HYBRID NOMA-ZFP SCHEMES

To highlight the performance of the proposed MA scheme, numerical results are presented for the case of a four-cell VLC network, as illustrated in Fig. 2.

A. PERFORMANCE METRICS

The network sum-rate, i.e., the maximum achievable total throughput, as well as the fairness criterion are taken as performance metrics in this work. To calculate the sum-rate, we use (12) and (13) to calculate the SINR and the achievable throughput for CCUs, respectively. For CEUs, assuming perfect removal of CCU signals by SIC, the SNR and the achievable throughput are calculated from (8) and (9), respectively. Concerning the fairness metric, the *Jain's fairness index*, denoted FI, is used to provide an indication of the homogeneity of user performance across the network [44], and has the advantage of being a simple quantitative measure [45]. For N_r users, FI is defined as

$$\text{FI} = \frac{\left(\sum_{j=1}^{N_r} R_j\right)^2}{N_r \sum_{j=1}^{N_r} R_j^2}, \tag{28}$$

where R_j is the upper bound on the throughput of U_j. When all users achieve the same upper bound on their data rate, the denominator equals $N_r(N_r R_j^2)$, resulting in FI $= 1$. As the difference between these bounds increases, FI decreases. The interest of FI in this study is that it jointly considers the homogeneity of data rates of both CCUs and CEUs.

Compared with NOMA-ZFP-B, NOMA-ZFP-A has a much lower computational complexity for calculating $\boldsymbol{W}$. Given the aforementioned optimization criteria, we expect that NOMA-ZFP-A provides a better FI (especially for relatively low SNRs), whereas NOMA-ZFP-B should provide a higher sum-rate (see Section IV-C).

TABLE 1. Simulation parameters.

Room dimension	(7 m × 7 m × 3 m)
LED luminaire Lamertian order m *	1
Number of LED chips per luminaire †	36
LED conversion efficiency $\mathcal{S}$ †	0.44 W/A
PD responsivity $\mathcal{R}$ ‡	0.4 A/W
PD area *	1 cm^2
Rx's FOV *	62 deg.
Refractive index of optical concentrator *	1.5
BW B	10 MHz
Equivalent Rx noise power spectral density ‡	10^{-21} A^2/Hz

* Adopted from [25]. ‡ Adopted from [14]. † Adopted from [27].

B. MAIN ASSUMPTIONS AND CONSIDERED SCENARIOS

The network considered in these studies mirrors the one used in [27] for the ease of comparison. In each configuration, within each cell, an LED luminaire acting as AP is placed at the center. Each luminaire is composed of 36 LED chips with conversion efficiency of $\mathcal{S} = 0.44$ W/A. Unless otherwise specified, we consider a drive current per LED chip of 100 mA, resulting in an emitting optical power of $P_o = 1.584$ W from each LED luminaire [27] (P_o is related to P_e through $P_o = \mathcal{S}\sqrt{P_e}$). The total number of users is set to 8 and different scenarios are considered with respect to their positions inside the room. The Rxs are assumed to be placed at 0.85 m above the floor level. Table 1 summarizes the simulation parameters. Note that, though the presented numerical results depend on the particular parameters chosen, higher data rates can be possible with wider bandwidth LEDs or greater Tx power. The presented analysis and conclusions can be generalized to other scenarios.

Figure 3 illustrates the three scenarios considered, showing the specific locations of the users and the APs, and the cell boundaries. Note that we will present later at the end of Section IV-C a more general study by considering 100 randomly generated scenarios.

In all considered scenarios, there is a single CEU in the coverage area of two adjacent cells. In Scenario 1 (in Fig. 3(a)), users are nearly equally distributed within the cells, such that each cell has in its coverage one CCU. In Scenario 2 (in Fig. 3(b)), Cell 4 has no CCU, Cell 3 has two CCUs, and the other two cells have one CCU. Lastly, in Scenario 3 (in Fig. 3(c)), Cells 2 and 4 have no CCUs, and the two other cells have two CCUs. The same locations and numbers of CEUs are considered for all scenarios, which are specified in Table 2, together with the locations of APs and those of CCUs according to the different considered scenarios. These are chosen to represent an increase in complexity from Scenario 1 to Scenario 3, by increasing the irregularity of users' distribution within the cells. The different locations of CCUs also allows for the investigation of the performance of the developed NOMA-ZFP algorithms in a variety of environments.

Note that, given the advantage of NOMA-ZFP in dealing with ICI compared with conventional NOMA, in the considered scenarios we have intentionally considered CEUs as being in the coverage area of only two APs. In fact, when

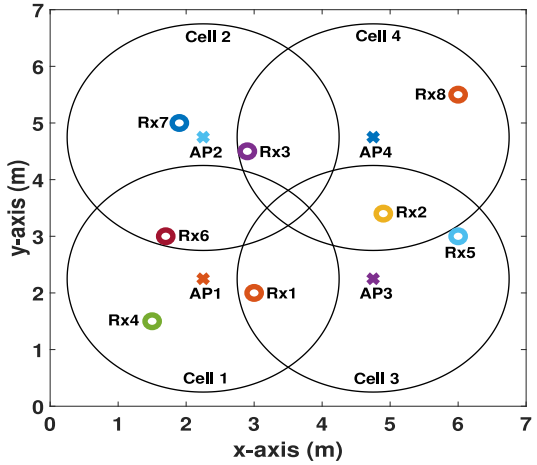

(a) Scenario 1

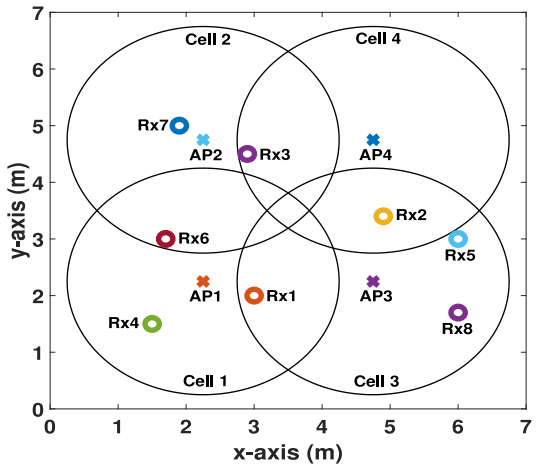

(b) Scenario 2

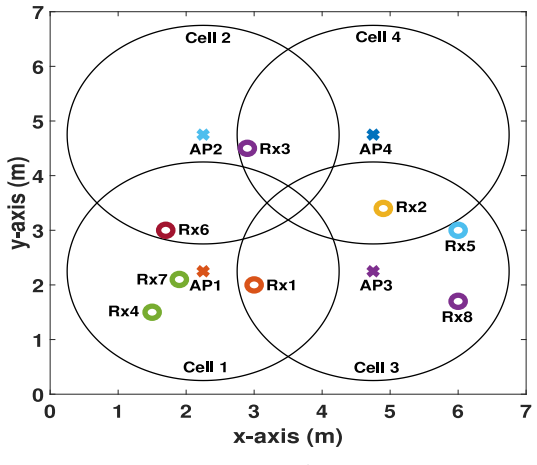

(c) Scenario 3

FIGURE 3. Illustration of top view of the considered scenarios: × and ∘ represent AP and user locations, respectively.

a CEU is placed in the intersection of three or four APs, this will result in a considerably degraded performance for NOMA-A and NOMA-B schemes. Indeed, for NOMA-A, this will increase the number of users handled by the corresponding APs, resulting in less resources available per user. For NOMA-B, those CEUs will be severely penalized due to receiving a high level of interference from the other APs. Here, we exclude such particular cases for which the hybrid approach will clearly outperform the NOMA-only approaches.

For the CCUs employing NOMA, we consider static PA with $\alpha = 0.3$, which was verified through simulations to make the best compromise between the sum-rate and FI for Scenario 1. Concerning CEUs, we impose the quality-of-service (QoS) constraint on minimum achievable user rate of 5 Mbps, which in turn gives a constraint of a minimum SNR of 1 dB. Accordingly, the PA weight a_{CEU}^2 in the hybrid scheme is set to 6%, which was calculated for Scenario 1 so as to satisfy the QoS condition.

C. PERFORMANCE STUDY

Figure 4 shows the upper bounds on the throughput of different users in the three considered scenarios and with the four MA schemes of NOMA-A, NOMA-B, NOMA-ZFP-A, and NOMA-ZFP-B, defined in Sections II-D and III-B.

The performance of several particular users are highlighted in the following in order to provide a deeper interpretation of the results in Fig. 4. For the sake of clarification, Table 3 lists the decoding order in detecting users' signals (ascending order) for the case of NOMA-A.

- *Case of Rx2:* In Scenario 1, this user attains a much higher throughput with NOMA-A, compared with NOMA-B, in particular. By referring to Table 3, the decoding order for Rx2 in both cells 3 and 4 is the largest, which means it detects its signal after the other users and hence can remove their interference using SIC. In Scenarios 2 and 3, Rx2 achieves a higher throughput with NOMA-ZFP-B because the whole power of AP 4 is allocated to the CEUs as there is no CCU in Cell 4.
- *Case of Rx7:* In Scenario 1, NOMA-A and NOMA-B provide a much better performance, compared to the hybrid schemes. In particular, with NOMA-B, a smaller number of users are handled by AP 2 (compared with the NOMA-A case) and, consequently, this AP has more power resources available per user. In addition, Rx7 has the highest decoding order (permitting interference removal using SIC), resulting in the relatively high throughput for this user. For the same reasons, Rx7 has still a superior performance in Scenarios 2 and 3 with NOMA-A and NOMA-B, as compared to the hybrid schemes.
- *Case of Rx8 in Scenario 1:* We notice a much higher throughput for this user with NOMA-B. Here Rx2 and Rx3 are associated with the AP 3 and AP 2, respectively, which leads to allocating all the AP 4 power to Rx8. As a result, Rx8 is the only effective user in Cell 4 having no interfering users.

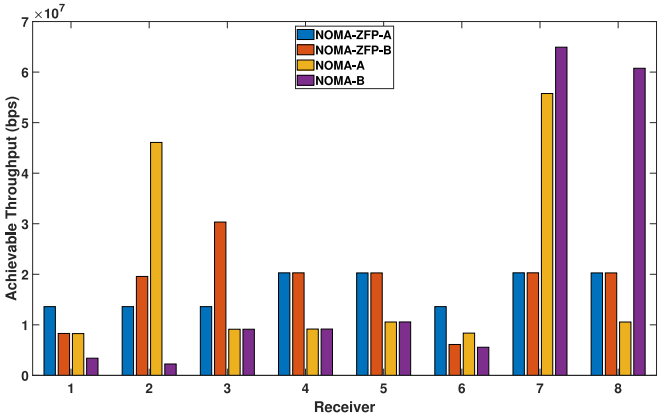

(a) Scenario 1

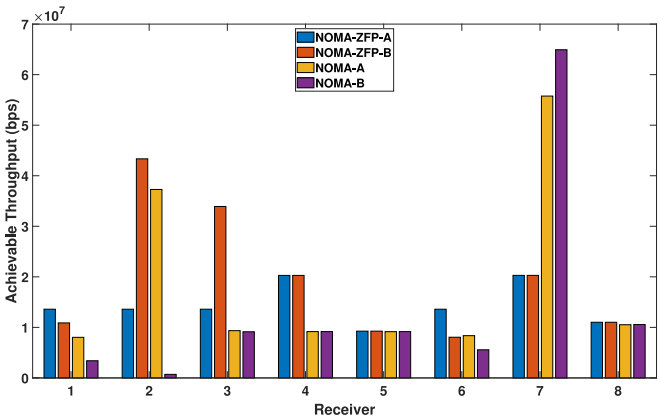

(b) Scenario 2

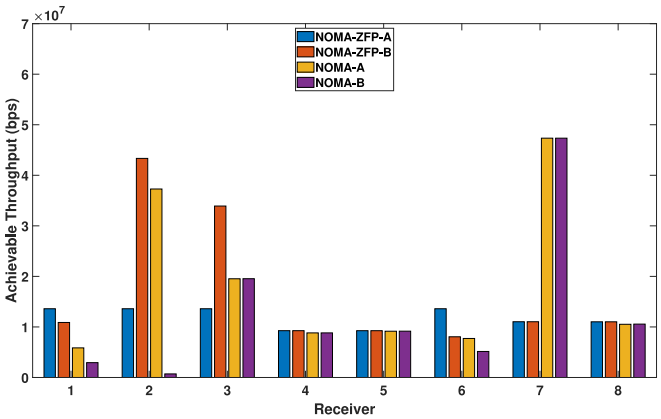

(c) Scenario 3

FIGURE 4. Upper bounds on the achieved rates for the users with NOMA-A, NOMA-B, NOMA-ZFP-A, and NOMA-ZFP-B schemes for the three considered scenarios in Fig. 3; $P_O = 1.584$ W. (a) Scenario 1 (b) Scenario 2 (c) Scenario 3.

- *Case of Rx3 in Scenario 3:* This user attains almost the same throughput with NOMA-A and NOMA-B. In fact, although Rx3 is the only user in Cell 2 with NOMA-B, which leads to more received power from AP 2, this is associated with more interference from AP 4.

Figure 5 presents the FI for the achievable network throughput in the three considered scenarios. Notice that

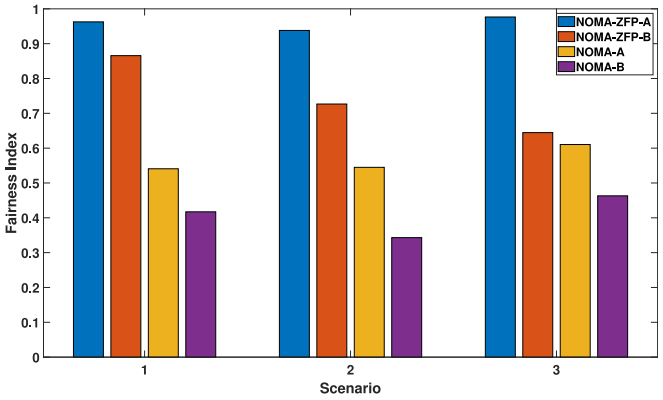

FIGURE 5. Network FI comparison for the considered MA schemes; $P_O = 1.584$ W.

NOMA-ZFP-A and NOMA-ZFP-B outperform the two other MA schemes in all scenarios. The reason of this advantage is three-fold: (i) having a smaller number of only-NOMA-associated users in the cells (i.e., without ZF pre-coding), which allows a better utilization of the resources to achieve a better individual performance for the users; (ii) benefiting from the broadcast feature of the MU-MISO, which allows allocating a small portion of the total available power in each AP to achieve an acceptable performance for CEUs, while decreasing the interference caused by CEU signals on CCUs; and (iii) exploiting SIC for canceling the interference arising from CCU signals on CEUs. Meanwhile, notice an improved performance in terms of fairness for NOMA-ZFP-A, as compared with NOMA-ZFP-B for all scenarios, which is due to the optimization criterion used for the former, as described in Section III-B. Also, NOMA-A outperforms NOMA-B since it ensures a more uniform performance for the users by decreasing the ICI effect for CEUs.

We have further compared the total network throughput, i.e., sum-rate, of the four MA schemes in Fig. 6 for the three scenarios, which is calculated using (9) and (13). Notice that NOMA-B has the maximum performance in Scenario 1 since every Rx is associated with only one AP (see Fig. 3), which globally results in increased power per user for each AP. The opposite situation arises in Scenarios 2 and 3 where the association with only one AP penalizes NOMA-B. For instance, Cell 4 has no CCU to serve and the CEUs are associated with the nearest AP, which results in wasting the resources of AP 4. We notice that NOMA-ZFP-B offers a better performance for Scenario 2, compared with NOMA-A, whereas the latter outperforms it for Scenarios 1 and 3. Indeed, the users corresponding to the highest channel gains in NOMA-A are allocated the smallest PA weight. These users benefit from SIC for removing the interference, which is not the case with NOMA-ZFP-B. Among NOMA-ZFP-A and NOMA-ZFP-B, the latter provides a superior performance in all scenarios, which is due to the optimization criterion used for calculating the pre-coding weights $\boldsymbol{W}$.

For the sake of completeness and to better see the advantage of the ZFP-based schemes, we have contrasted in Fig. 7

TABLE 2. Locations of APs, CCUs, and CEUs (in meter) in the considered scenarios.

Scenario	APs locations: AP1, AP2, AP3, AP4
1, 2, 3	(2.25, 2.25, 2.5), (2.25, 4.75, 2.5), (4.75, 2.25, 2.5), (4.75, 4.75, 2.5)
Scenario	CCUs locations: Rx4, Rx5, Rx7, Rx8
1	(1.5, 1.5, 0.85), (6, 3, 0.85), (1.9, 5, 0.85), (6, 5.5, 0.85)
2	(1.5, 1.5, 0.85), (6, 3, 0.85), (1.9, 5, 0.85), (6, 1.7, 0.85)
3	(1.5, 1.5, 0.85), (6, 3, 0.85), (1.9, 2.1, 0.85), (6, 1.7, 0.85)
Scenario	CEUs locations: Rx1, Rx2, Rx3, Rx6
1, 2, 3	(3, 2, 0.85), (4.9, 3.4, 0.85), (2.9, 4.5, 0.85), (1.7, 3, 0.85)

TABLE 3. Decoding order of users' signals for NOMA-A (ascending).

Scenario	Cell 1	Cell 2	Cell 3	Cell 4
1	Rx4 - Rx6 - Rx1	Rx6 - Rx3 - Rx7	Rx1 - Rx5 - Rx2	Rx3 - Rx8 - Rx2
2	Rx4 - Rx6 - Rx1	Rx6 - Rx3 - Rx7	Rx1 - Rx5 - Rx8 - Rx2	Rx3 - Rx2
3	Rx4 - Rx6 - Rx1 - Rx7	Rx6 - Rx3	Rx1 - Rx5 - Rx8 - Rx2	Rx3 - Rx2

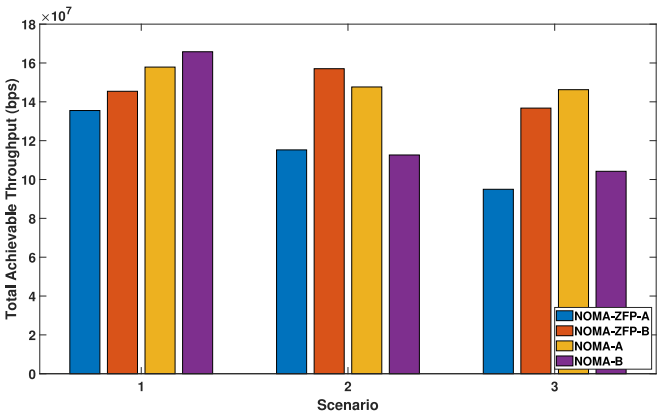

FIGURE 6. Network sum-rate comparison for the considered MA schemes; $P_O = 1.584$ W.

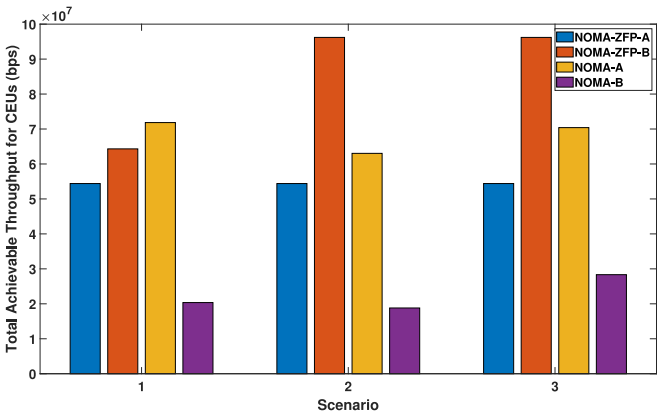

FIGURE 7. Comparison between the total achieved throughput of CEUs for the considered MA schemes; $P_O = 1.584$ W.

the total achievable data rates for the CEUs. As expected, NOMA-B offers the worst performance, because with this scheme, CEUs are affected by the interference they receive from the other APs (other than their main AP), resulting in degraded SINR and hence decreased throughput. We notice that in Scenarios 2 and 3, NOMA-ZFP-B offers the best performance. In fact, while ensuring a target performance for CEUs (here we imposed the QoS requirement of at least 5 Mbps data rate per user) using a fraction of the available power in each AP (see Section IV-B), NOMA-ZFP-B benefits from the broadcast feature of the MU-MISO, while minimizing the interference caused by the CCUs signals using SIC. For Scenario 1, however, NOMA-A outperforms NOMA-ZFP-B, because the former benefits from a high throughput of Rx2, due to the smallest decoding order in Cells 3 and 4 (see Table 3), allowing interference cancellation by SIC. Note that this is not the case for Scenarios 2 and 3 where with NOMA-ZFP-B, the entire AP 4 power is allocated to CEUs (there is no CCU in Cell 4). Also, a higher throughput is obtained with NOMA-ZFP-B, compared to NOMA-ZFP-A, which is again due to the optimization criteria considered.

Lastly, the effect of increasing the transmitted optical power P_o on the network sum-rate and FI is considered in the three scenarios. Results are shown in Figs. 8 and 9 for $P_o = 5$ and 10 W, while (as before) we have considered allocating 6% of the electrical power to CEUs. Note that the increase in P_o can be achieved by adding more LEDs to a luminaire, for instance. Indeed, we expect that with increased P_o, better performance can be achieved for CEUs (as they perform SIC for interference cancellation), and the proposed hybrid schemes become even more advantageous. Notice from Fig. 8 that, with increased P_o, NOMA-ZFP-B outperforms NOMA-A and NOMA-B in all scenarios regarding the network sum-rate, and that the performance of NOMA-ZFP-A also improves with respect to these latter. Furthermore, from Fig. 9, at higher values of P_o, the hybrid schemes outperform NOMA-A and NOMA-B in all scenarios regarding FI. Note that similar conclusions can be drawn for the case of changing the Rx height, which will affect the received power.

In all previously-presented results, we considered the three special scenarios of Fig. 3. Although the rationale behind considering these cases was explained (see Section IV-B), it would be interesting to see the performance of the proposed hybrid methods on average. For this purpose, we have considered randomly generated users' locations within the 4-cell room (of the same dimensions as in Fig. 3). The optical power corresponding to each AP is set to $P_o = 1.584$ W. The average sum-rate and FI are presented in Table 4, which correspond to a total of 100 scenarios (selected among about

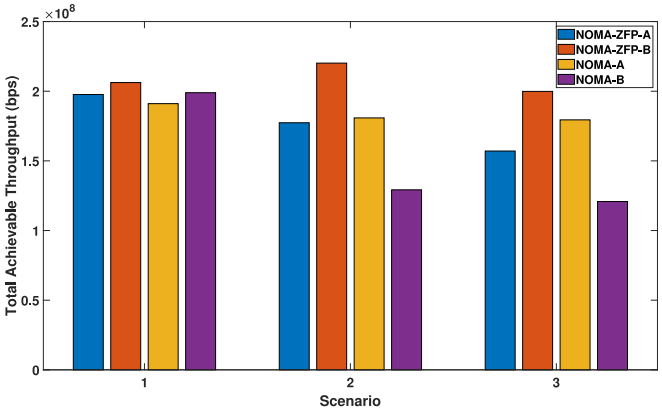

(a) $P_o = 5$ W

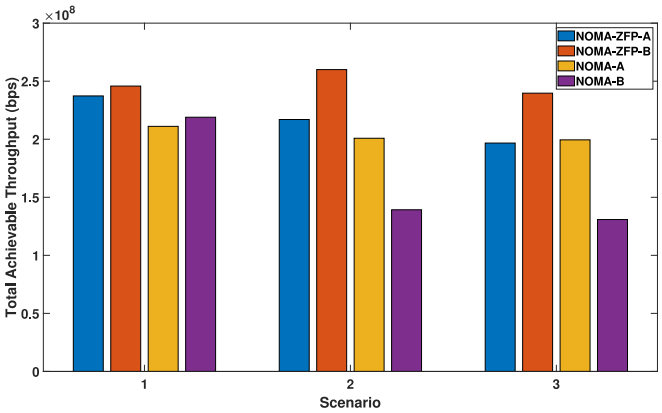

(b) $P_o = 10$ W

FIGURE 8. Comparison of network sum-rate for the different MA schemes for transmitted optical powers of 5 and 10 W.

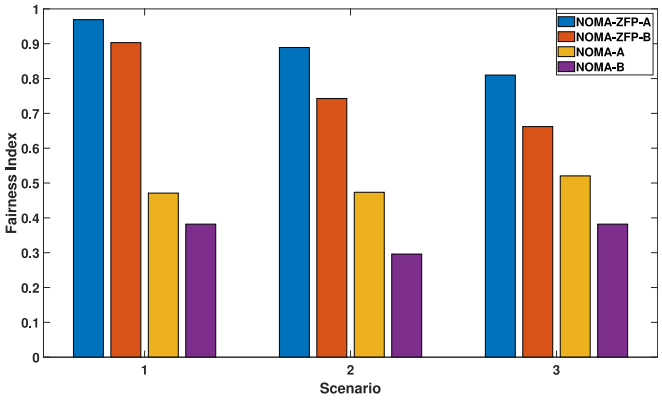

(a) $P_o = 5$ W

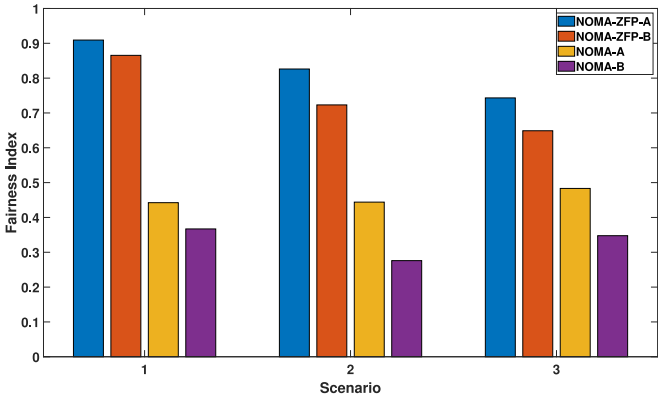

(b) $P_o = 10$ W

FIGURE 9. Comparison of network FI of the different MA schemes for $P_O = 5$ and 10 W.

1000 randomly-generated locations for eight users), satisfying the existence of four CEUs, with each CEU being in the coverage area of only two APs. From these results, we notice that, in general, the proposed hybrid schemes outperform the NOMA-based ones in average FI, whereas the latter achieve a better average sum-rate performance. Also, NOMA-ZFP-B outperforms NOMA-ZFP-A in average sum-rate, as shown in the already-presented results (see Figs. 6 and 8). Concerning the average FI, these results attest the same trend in Figs. 5 and 9, i.e., NOMA-ZFP-A achieves the best performance, followed by NOMA-ZFP-B, while NOMA-A outperforming NOMA-B.

To study the relationship between the network sum-rate and fairness for NOMA-ZFP-A and -B schemes, we have shown in Fig. 10 the effect of varying the percentage of the power allocated to CEUs (i.e., a^2_{CEU}) on the average total achievable throughput of CCUs and CEUs, as well as on the average network sum-rate and fairness. To obtain these results, 100 random scenarios were considered with the same conditions as for the results presented in Table 4. The results of Fig. 10(a) are in accordance with those in Figs. 6 and 7, where we notice that, with decrease in a^2_{CEU}, the average throughput of CEUs degrades, unlike that of CCUs. The presented plots have almost the same slope for the two NOMA-ZFP schemes. However, we have a higher throughput for CEUs for NOMA-ZFP-B, which is due to the considered criteria for calculating $\boldsymbol{W}$ (see Section III-B). Considering now Fig. 10(b), we see a decrease in the average network sum-rate with increase in a^2_{CEU} due to the decrease in CCUs power. At the same time, this results in a better fairness, as the throughputs of CEUs approach those of CCUs. Interestingly, for NOMA-ZFP-B, there is an optimal value for a^2_{CEU} (here, 4%) beyond which the fairness degrades, because the throughputs of CEUs dominate the sum-rate and exceed considerably those of CCUs.[4]

D. COMPUTATIONAL COMPLEXITY AND NETWORK LATENCY

For the sake of completeness, we discuss here the computational complexity of the considered MA schemes at the Tx and the Rx, as well as the overall network latency.

As concerns the computational complexity at the Tx, for NOMA-ZFP schemes, it mainly depends on:

4. The optimum a^2_{CEU} is around 13% for NOMA-ZFP-A, which is not shown in Fig. 10 for the sake of presentation clarity. This optimum is smaller for NOMA-ZFP-B due to the criterion of throughput optimization for this scheme.

TABLE 4. Sum-rate and FI performance averaged over 100 random scenarios.

	NOMA-ZFP-A	NOMA-ZFP-B	NOMA-A	NOMA-B
Average sum-rate (bps)	1.12×10^8	1.41×10^8	1.67×10^8	1.79×10^8
Average FI	0.83	0.75	0.52	0.46

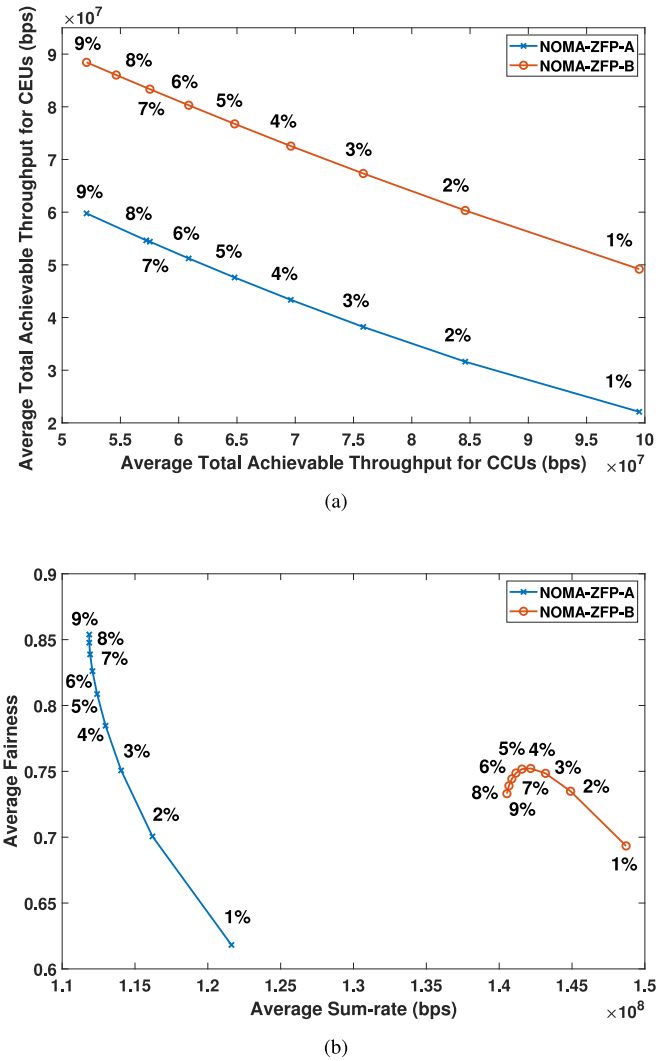

FIGURE 10. Comparison between (a) average achievable throughput for CCUs and CEUs; and (b) average network sum-rate and fairness for NOMA-ZFP-A and NOMA-ZFP-B schemes, for different percentages of power allocated to CEUs, a^2_{CEU}.

- Complexity of ZF pre-coding, which mainly concerns matrix multiplication and inversion, and is given by $O(2N^2_{\text{CEU}}N_t + N^3_{\text{CEU}})$ [46];
- Complexity of NOMA resource allocation (remember that here we consider the simple static power allocation, which is of very low complexity);
- Complexity of calculating the optimal $\boldsymbol{W}$, which depends on the target criterion (e.g., throughput maximization for NOMA-ZFP-B). This complexity is much higher for NOMA-ZFP-B compared to NOMA-ZFP-A, since the former uses convex optimization for calculating $\boldsymbol{W}$, with complexity varying depending on the number of iterations needed for the interior point method to converge to the solution in CVX;
- Complexity of acquiring CSI, where NOMA-ZFP schemes add more complexity to the system.

For NOMA schemes, the computational complexity depends on the resource allocation process. In the considered NOMA and NOMA-ZFP schemes, the complexity of NOMA resource allocation is negligible, as only static power allocation is considered. For this reason, the computational complexity of NOMA schemes is much lower than that of NOMA-ZFP schemes. In addition, NOMA-B has a lower complexity than NOMA-A, as the complexity of resource allocation increases by increased number of users.

Concerning the computational complexity at the Rx side, for NOMA-ZFP schemes, it mainly depends on the complexity of SIC detection. The number of SIC steps needed for both NOMA-ZFP-A and NOMA-ZFP-B equals $\sum_{i=1}^{N_t}\sum_{k=1}^{N_{\text{CCU},i}-1} k + N_{\text{CEU}}\sum_{i=1}^{N_t} N_{\text{CCU},i}$, where the first and the second terms denote the number of SIC steps needed by CCUs and CEUs, respectively. For NOMA schemes, the number of SIC steps equals $\sum_{i=1}^{N_t}\sum_{k=1}^{N_{r,i}-1} k$, where $N_{r,i}$ is the number of users handled by AP_i. In general, we have a larger $N_{r,i}$ for NOMA-A due to handling of each CEU by multiple APs, resulting in a higher complexity, compared with NOMA-B. Here again, NOMA-ZFP schemes have a higher complexity, compared to NOMA.

Concerning network latency, whatever the MA scheme, the main factors include Tx/Rx computational complexity, handovers, and CSI requirement. Although NOMA-ZFP schemes have a higher computational complexity, they have a significant advantage over NOMA in terms of handovers. This is because handling of CEU signals by ZF pre-coding decreases the handover rate in the network. Lastly, for both NOMA and NOMA-ZFP schemes, the CSI of all users is required by the corresponding APs. The main difference is that in NOMA-ZFP, CEUs require the CSI of the users in all cells, which requires the exchange of CSI between all APs through the central control unit, involving hence a slight additional latency.

V. CONCLUSION AND DISCUSSION

In this paper, two novel hybrid NOMA-ZFP schemes were proposed for multi-cell VLC networks. The proposed schemes are based on using NOMA for handling CCUs while exploiting the MU-MISO structure of the VLC networks with multiple luminaires (acting as APs) to serve CEUs using ZF pre-coding. Using the proposed MA schemes, a relatively small fraction of the total available power at the APs is allocated to CEUs, causing rather low interference on CCUs, and allowing reduced complexity of NOMA signaling for CCUs. These schemes are compared with two available NOMA schemes in the literature considering three MA scenarios with different complexity and irregularity of the user

distribution within the cells. The advantages of NOMA-ZFP are demonstrated in terms of sum-rate (i.e., the upper bound on the total network achievable data rate) and fairness, in particular, in relatively high-SNR regimes.

Among the two proposed hybrid solutions, NOMA-ZFP-B has a much higher computational complexity because of the requirement for convex optimization to compute the pre-coding coefficients $\boldsymbol{W}$. NOMA-ZFP-A, however, can be considered as a good compromise between performance and complexity. Based on the results presented for relatively low and high optical powers, the proposed hybrid schemes can be considered as good candidates for applications using light dimming as they offer a robust performance (in terms of both network fairness and sum-rate) over a wide range of transmit optical powers.

The performance improvement of the proposed hybrid schemes is achieved at the price of an increased overall complexity of the network, as compared to the classical NOMA schemes, since it necessitates the cooperation of the APs (via the central control unit) in handling CEUs. In particular, the CSI of all CEUs should be provided at the APs in order to do pre-coding. In addition, the CSI of all CCUs in the neighboring cells is required for the CEUs to perform SIC to remove IUI from the corresponding CCUs before detecting their own signal. In order to reduce the computational load at the APs, CSIs of all CCUs and CEUs can be sent from the APs to the central control unit (see Fig. 1), where the processing of the different users signals will be done. Note that, since CEUs rely on ZF pre-coding for accessing their signals, their performance can be affected by the correlation between the CEUs' channels.

Lastly, for very large indoor spaces, broadcasting the signals for CEUs from all APs does not appear to be efficient. Indeed, APs that are too far from the actual CEU position, will likely have a negligible impact on the user. Therefore, to reduce the network complexity under such conditions, a more appropriate methodology consists of broadcasting the CEUs' signals by only neighboring cell APs. At the same time, the number of "broadcasting APs" should be determined based on the maximum number of CEUs that have to be handled in the network, because for linear ZF pre-coding we have the strict condition that the number of Txs (i.e., APs) should be larger than or equal to the number of Rxs (i.e., CEUs).

Future work will also investigate the effect of outdated CSI, the interest of user grouping and optimal PA (rather than static PA, considered here), as well as the use of other criteria for resource allocation in the proposed hybrid MA scheme, in order to further improve the network performance.

REFERENCES

[1] Z. Ghassemlooy, L. N. Alves, S. Zvànovec, and M. A. Khalighi, Eds., *Visible Light Communications: Theory and Applications*. Boca Raton, FL, USA: CRC Press, 2017.

[2] S. Wu, H. Wang, and C. Youn, "Visible light communications for 5G wireless networking systems: From fixed to mobile communications," *IEEE Netw.*, vol. 28, no. 6, pp. 41–45, Nov./Dec. 2014.

[3] A. R. Ndjiongue, T. M. N. Ngatched, O. A. Dobre, and A. G. Armada, "VLC-based networking: Feasibility and challenges," *IEEE Netw.*, early access, Jan. 27, 2020, doi: 10.1109/MNET.001.1900428.

[4] Z. Ding, Z. Yang, P. Fan, and H. V. Poor, "On the performance of non-orthogonal multiple access in 5G systems with randomly deployed users," *IEEE Signal Process. Lett.*, vol. 21, no. 12, pp. 1501–1505, Dec. 2014.

[5] L. Dai, B. Wang, Y. Yuan, S. Han, C. I, and Z. Wang, "Non-orthogonal multiple access for 5G: Solutions, challenges, opportunities, and future research trends," *IEEE Commun. Mag.*, vol. 53, no. 9, pp. 74–81, Sep. 2015.

[6] Z. Ding, M. Peng, and H. V. Poor, "Cooperative non-orthogonal multiple access in 5G systems," *IEEE Commun. Lett.*, vol. 19, no. 8, pp. 1462–1465, Aug. 2015.

[7] Z. Ding *et al.*, "Application of non-orthogonal multiple access in LTE and 5G networks," *IEEE Commun. Mag.*, vol. 55, no. 2, pp. 185–191, Feb. 2017.

[8] M. D. Soltani, X. Wu, M. Safari, and H. Haas, "Bidirectional user throughput maximization based on feedback reduction in LiFi networks," *IEEE Trans. Commun.*, vol. 66, no. 7, pp. 3172–3186, Jul. 2018.

[9] R. C. Kizilirmak, C. R. Rowell, and M. Uysal, "Non-orthogonal multiple access (NOMA) for indoor visible light communications," in *Proc. Int.Workshop Opt. Wireless Commun. (IWOW)*, Istanbul, Turkey, Sep. 2015, pp. 98–101.

[10] Y. Liu, Z. Qin, M. Elkashlan, Z. Ding, A. Nallanathan, and L. Hanzo, "Nonorthogonal multiple access for 5G and beyond," *Proc. IEEE*, vol. 105, no. 12, pp. 2347–2381, Dec. 2017.

[11] H. Marshoud, V. M. Kapinas, G. K. Karagiannidis, and S. Muhaidat, "Non-orthogonal multiple access for visible light communications," *IEEE Photon. Technology Lett.*, vol. 28, no. 1, pp. 51–54, Jan. 2016.

[12] S. Al-Ahmadi, O. Maraqa, M. Uysal, and S. M. Sait, "Multi-user visible light communications: State-of-the-art and future directions," *IEEE Access*, vol. 6, pp. 70555–70571, 2018.

[13] X. Ling, J. Wang, Z. Ding, C. Zhao, and X. Gao, "Efficient OFDMA for LiFi downlink," *J. Lightw. Technol.*, vol. 36, no. 10, pp. 1928–1943, May 15, 2018.

[14] L. Yin, W. O. Popoola, X. Wu, and H. Haas, "Performance evaluation of non-orthogonal multiple access in visible light communication," *IEEE Trans. Commun.*, vol. 64, no. 12, pp. 5162–5175, Dec. 2016.

[15] M. W. Eltokhey, M. A. Khalighi, and Z. Ghassemlooy, "Multiple access techniques for VLC in large space indoor scenarios: A comparative study," in *Proc. 15th Int. Conf. Telecommun. (ConTEL)*, Graz, Austria, Jul. 2019, pp. 1–6.

[16] H. Marshoud, P. C. Sofotasios, S. Muhaidat, G. K. Karagiannidis, and B. S. Sharif, "On the performance of visible light communication systems with non-orthogonal multiple access," *IEEE Trans. Wireless Commun.*, vol. 16, no. 10, pp. 6350–6364, Oct. 2017.

[17] C. Chen, S. Videv, D. Tsonev, and H. Haas, "Fractional frequency reuse in DCO-OFDM-based optical attocell networks," *J. Lightw. Technol.*, vol. 33, no. 19, pp. 3986–4000, Oct. 1, 2015.

[18] X. Zhang, Q. Gao, C. Gong, and Z. Xu, "User grouping and power allocation for NOMA visible light communication multi-cell networks," *IEEE Commun. Lett.*, vol. 21, no. 4, pp. 777–780, Apr. 2017.

[19] K. Zhou, C. Gong, and Z. Xu, "Color planning and intercell interference coordination for multicolor visible light communication networks," *J. Lightw. Technol.*, vol. 35, no. 22, pp. 4980–4993, Nov. 15, 2017.

[20] C. Chen, W. Zhong, H. Yang, S. Zhang, and P. Du, "Reduction of SINR fluctuation in indoor multi-cell VLC systems using optimized angle diversity receiver," *J. Lightw. Technol.*, vol. 36, no. 17, pp. 3603–3610, Sep. 1, 2018.

[21] J. Shi, J. He, K. Wu, and J. Ma, "Enhanced performance of asynchronous multi-cell VLC system using OQAM/OFDM-NOMA," *J. Lightw. Technol.*, vol. 37, no. 20, pp. 5212–5220, Oct. 15, 2019.

[22] Y. Fu, Y. Hong, L. Chen, and C. W. Sung, "Enhanced power allocation for sum rate maximization in OFDM-NOMA VLC systems," *IEEE Photon. Technol. Lett.*, vol. 30, no. 13, pp. 1218–1221, Jul. 1, 2018.

[23] H. Shen, Y. Deng, W. Xu, and C. Zhao, "Rate-maximized zero-forcing beamforming for VLC multiuser MISO downlinks," *IEEE Photon. J.*, vol. 8, no. 1, pp. 1–13, Feb. 2016.

[24] B. Li, J. Wang, R. Zhang, H. Shen, C. Zhao, and L. Hanzo, "Multiuser MISO transceiver design for indoor downlink visible light communication under per-LED optical power constraints," *IEEE Photon. J.*, vol. 7, no. 4, pp. 1–15, Aug. 2015.

[25] Z. Yu, R. J. Baxley, and G. T. Zhou, "Multi-user MISO broadcasting for indoor visible light communication," in *Proc. Int. Conf. Acoust. Speech Signal Process. (ICASSP)*, Vancouver, BC, Canada, May 2013, pp. 4849–4853.

[26] T. V. Pham, H. Le-Minh, and A. T. Pham, "Multi-user visible light communication broadcast channels with zero-forcing precoding," *IEEE Trans. Commun.*, vol. 65, no. 6, pp. 2509–2521, Jun. 2017.

[27] H. Ma, L. Lampe, and S. Hranilovic, "Coordinated broadcasting for multiuser indoor visible light communication systems," *IEEE Trans. Commun.*, vol. 63, no. 9, pp. 3313–3324, Sep. 2015.

[28] X. Li, R. Zhang, J. Wang, and L. Hanzo, "Cell-centric and user-centric multi-user scheduling in visible light communication aided networks," in *Proc. IEEE Int. Conf. Commun. (ICC)*, London, U. K., Jun. 2015, pp. 5120–5125.

[29] V. Nguyen, H. D. Tuan, T. Q. Duong, H. V. Poor, and O. Shin, "Precoder design for signal superposition in MIMO-NOMA multicell networks," *IEEE J. Sel. Areas Commun.*, vol. 35, no. 12, pp. 2681–2695, Dec. 2017.

[30] W. Shin, M. Vaezi, B. Lee, D. J. Love, J. Lee, and H. V. Poor, "Non-orthogonal multiple access in multi-cell networks: Theory, performance, and practical challenges," *IEEE Commun. Mag.*, vol. 55, no. 10, pp. 176–183, Oct. 2017.

[31] L. Yin, X. Wu, and H. Haas, "SDMA grouping in coordinated multipoint VLC systems," in *Proc. IEEE Summer Topicals Meeting Series (SUM)*, Nassau, Bahamas, Jul. 2015, pp. 169–170.

[32] T. V. Pham, H. L. Minh, and A. T. Pham, "Multi-cell VLC: Multi-user downlink capacity with coordinated precoding," in *Proc. IEEE Int. Conf. Commun. Workshops (ICC Workshops)*, Paris, France, May 2017, pp. 469–474.

[33] Z. Feng, C. Guo, Z. Ghassemlooy, and Y. Yang, "The spatial dimming scheme for the MU-MIMO-OFDM VLC system," *IEEE Photon. J.*, vol. 10, no. 5, pp. 1–13, Oct. 2018.

[34] T. Komine and M. Nakagawa, "Fundamental analysis for visible-light communication system using led lights," *IEEE Trans. Consum. Electron.*, vol. 50, no. 1, pp. 100–107, Feb. 2004.

[35] K. Lee, H. Park, and J. R. Barry, "Indoor channel characteristics for visible light communications," *IEEE Commun. Lett.*, vol. 15, no. 2, pp. 217–219, Feb. 2011.

[36] S. Long, M. A. Khalighi, M. Wolf, S. Bourenanne, and Z. Ghassemlooy, "Investigating channel frequency selectivity in indoor visible-light communication systems," *IET Optoelectron.*, vol. 10, no. 3, pp. 80–88, Jun. 2016.

[37] J. M. Kahn and J. R. Barry, "Wireless infrared communications," *Proc. IEEE*, vol. 85, no. 2, pp. 265–298, Feb. 1997.

[38] M.-A. Khalighi, S. Long, S. Bourennane, and Z. Ghassemlooy, "PAM- and CAP-based transmission schemes for visible-light communications," *IEEE Access*, vol. 5, pp. 27002–27013, 2017.

[39] C. Chen, W. Zhong, H. Yang, and P. Du, "On the performance of MIMO-NOMA-based visible light communication systems," *IEEE Photon. Technol. Lett.*, vol. 30, no. 4, pp. 307–310, Feb. 15, 2018.

[40] Z. Yang, W. Xu, and Y. Li, "Fair non-orthogonal multiple access for visible light communication downlinks," *IEEE Wireless Commun. Lett.*, vol. 6, no. 1, pp. 66–69, Feb. 2017.

[41] S. Feng, R. Zhang, W. Xu, and L. Hanzo, "Multiple access design for ultra-dense VLC networks: Orthogonal vs non-orthogonal," *IEEE Trans. Commun.*, vol. 67, no. 3, pp. 2218–2232, Mar. 2019.

[42] M. Grant and S. Boyd. (Mar. 2014). *CVX: MATLAB Software for Disciplined Convex Programming, Version 2.1*. [Online]. Available: http://cvxr.com/cvx

[43] M. Grant and S. Boyd, "Graph implementations for nonsmooth convex programs," in *Recent Advances in Learning and Control* (Lecture Notes in Control and Information Sciences), V. Blondel, S. Boyd, and H. Kimura, Eds. London, U.K.: Springer, 2008, pp. 95–110.

[44] R. K. Jain, D.-M. W. Chiu, and W. R. Hawe, *A Quantitative Measure of Fairness and Discrimination for Resource Allocation in Shared Computer System*. Hudson, MA, USA: Eastern Res. Lab., 1984.

[45] H. Shi, R. V. Prasad, E. Onur, and I. G. M. M. Niemegeers, "Fairness in wireless networks:Issues, measures and challenges," *IEEE Commun. Surveys Tuts.*, vol. 16, no. 1, pp. 5–24, 1st Quart., 2014.

[46] R. Wang *et al.*, "Linear transceiver designs for MIMO indoor visible light communications under lighting constraints," *IEEE Trans. Commun.*, vol. 65, no. 6, pp. 2494–2508, Jun. 2017.

MAHMOUD WAFIK ELTOKHEY (Member, IEEE) received the B.Sc. and M.Sc. degrees from the Department of Electronics and Communications Engineering, Mansoura University, Mansoura, Egypt, in 2012 and 2016, respectively. He is currently pursuing the Ph.D. degree with Institut Fresnel, École Centrale Marseille, Marseille, France. He was a Research Assistant with the Center for Photonics and Smart Materials, Zewail City of Science and Technology, Giza, Egypt, from 2012 to 2018. His current research interests include optical wireless communications and visible light communications.

MOHAMMAD ALI KHALIGHI (Senior Member, IEEE) received the Ph.D. degree in telecommunications from the Institut National Polytechnique de Grenoble, Grenoble, France, in 2002.

He is currently an Associate Professor with École Centrale Marseille, Marseille, France, and the Head of the Telecommunications and Antenna Processing Group, Fresnel Institute Research Laboratory. He was the Vice-Chair for WG2 of the FP7 IC1101 COST Action OPTICWISE (Optical Wireless Communications—An Emerging Technology). He is the Project Coordinator for the H2020 ITN MSCA VisIoN (Visible-light-based Interoperability and Networking) project. He has coedited the book *Visible Light Communications: Theory and Applications* (CRC Press, 2017). His main research interests include signal processing for wireless communication systems with an emphasis on the physical layer aspects of free-space, underwater, and indoor visible-light optical communications. He was the co-recipient of the 2019 Best Survey Paper Award of the IEEE Communications Society. He is currently serving as an Editor for the IEEE TRANSACTIONS ON COMMUNICATIONS and has served as an Associate Editor for *IET Electronics Letters* as well as the Guest Co-Editor for *Optik* (Elsevier).

ABDALLAH S. GHAZY was born in Giza, Egypt, in 1983. He received the B.S. degree in electrical engineering from Azher University, Cairo, Egypt, in 2007, and the M.Sc. degree from the Egypt–Japan University of Science and Technology, Alexandria, Egypt, in 2016. He is currently pursuing the Ph.D. degree with McMster University, Hamilton, ON, Canada. His research interests include optical communications, wireless communications, and heterogeneous communications networks.

STEVE HRANILOVIC (Senior Member, IEEE) received the B.A.Sc. degree (Hons.) in electrical engineering from the University of Waterloo, Canada, in 1997, and the M.A.Sc. and Ph.D. degrees in electrical engineering from the University of Toronto, Canada, in 1999 and 2003, respectively.

He is a Professor with the Department of Electrical and Computer Engineering, McMaster University, Hamilton, ON, Canada, and currently serves as the Associate Dean (Academic). From 2010 to 2011, he spent his research leave as a Senior Member, Technical Staff in Advanced Technology for Research in Motion, Waterloo, ON, Canada. He has authored the book *Wireless Optical Communication Systems* (New York: Springer, 2004). His research interests are in the areas of free-space and optical wireless communications, digital communication algorithms, and electronic and photonic implementation of coding and communication algorithms.

Dr. Hranilovic was awarded the Government of Ontario Early Researcher Award in 2006. In 2016, the title of University Scholar was conferred upon him by McMaster University. He is a Licensed Professional Engineer in the Province of Ontario. He has served as an Associate Editor for the *Journal of Optical Communications and Networking* and an Editor for the IEEE TRANSACTIONS ON COMMUNICATIONS in the area of Optical Wireless Communications.